Atmospheric Measurement Techniques Discussions

Airborne lidar reflectance measurements at 1.57 µm in support of the A-SCOPE mission for atmospheric CO_2

A. Amediek[1], A. Fix[1], G. Ehret[1], J. Caron[2,*], and Y. Durand[2]

[1]Deutsches Zentrum für Luft- und Raumfahrt (DLR) Oberpfaffenhofen, Institut
für Physik der Atmosphäre, 82234 Wessling, Germany
[2]ESA/ESTEC, Earth Observation Project Department, 2201 AZ Noordwijk, The Netherlands
[*]working as a contractor from RHEA System SA

Correspondence to: A. Amediek (axel.amediek@dlr.de)

Title Page

Abstract	Introduction
Conclusions	References
Tables	Figures

|◄ | ►|
| ◄ | ► |

Back | Close

Full Screen / Esc

Printer-friendly Version

Interactive Discussion

Abstract

The characteristics of the lidar reflectance of the Earth's surface is an important is-
sue for the IPDA lidar technique (integrated path differential absorption lidar) which is
the proposed method for the spaceborne measurement of atmospheric carbon diox-
ide within the framework of ESA's A-SCOPE project. Both, the absolute reflectance
of the ground and its variations have an impact on the measurement sensitivity. The
first aspect influences the instrument's signal to noise ratio, the second one can lead
to retrieval errors, if the ground reflectance changes are strong on small scales. The
investigation of the latter is the main purpose of this study. Airborne measurements
of the lidar ground reflectance at $1.57\,\mu$m wavelength were performed in Central and
Western Europe, including many typical land surface coverages as well as the open
sea. The analyses of the data show, that the lidar ground reflectance is highly variable
on a wide range of spatial scales. However, by means of the assumption of laser foot-
prints on the order of several tens of meters, as planned for spaceborne systems, and
by means of an averaging of the data it was shown, that this specific retrieval error is
compatible with the sensitivity requirements of spaceborne CO_2 measurements.

1 Introduction

A-SCOPE (Advanced Space Carbon and Climate Observation of Planet Earth) is one
of the six candidate Earth Explorer missions which have been selected by the Euro-
pean Space Agency (ESA) for assessment studies (ESA, 2008). This mission aims on
determination of regional sources and sinks of CO_2 by means of inverse modeling us-
ing global observations of XCO_2 (column-weighted dry-air mixing ratio of atmospheric
CO_2) in the near infrared spectral region (ESA, 2008). A-SCOPE will have its own
light source emitting pulsed narrow-line laser radiation either in the $1.6\,\mu$m or $2.0\,\mu$m
spectral range. It will use a range-gated receiver for distinguishing between the signals
backscattered from the Earth surface, clouds or elevated aerosol layers. The retrieval

of $X\text{CO}_2$ is based on the Integrated Path Differential Absorption (IPDA) lidar method which allows to measure the CO_2 Differential Atmospheric Optical Depth (DAOD) from top of the atmosphere down to the Earth's surface by comparing the lidar echoes at two transmitted wavelengths (e.g. termed as on- and off-line) in the vicinity of the selected

5   CO_2-absorption line (Ehret et al., 2008).

The random error characteristics of the measured DAOD and hence the quality of the retrieved $X\text{CO}_2$ values from A-SCOPE observations strongly depends on the type of surface. The surface reflectance characteristics are quite different for land and water. In general the reflectivity of the sea is caused by specular reflection on the water sur-

10 face, by backscattering due to whitecaps, and by subsurface backscattering (Menzies et al., 1998). As well-known from previous studies, over the ocean the lidar reflectance will strongly be anticorrelated to the surface wind speed which effects the possibility for specular reflectance leading to strong lidar echoes (Cox and Munk, 1954; Bufton et al., 1983). This is due to the slope probability distribution of sea waves which results in a

15 higher reflectivity in case of low wind speeds and vice versa (Cox and Munk, 1954). Due to the small penetration depth in water for wavelengths in the near IR around 1.6 μm, the magnitude of the diffuse (non-directional) scattering component on water particles is expected to be negligible compared to the glint (directional) reflectance given for the typical lidar geometry (Friedman, 1969). In contrast to the ocean, land

20 surfaces usually provide higher reflectance values, although the directional character-istic (e.g. hot spot over vegetation) is less pronounced (Baldridge et al., 2009; Bréon et al., 2002). However, the brightness of the various surface types can vary substantially for different wavelengths as shown for example by the results from 1.6 μm channel of the MODIS (moderate-resolution imaging spectrometer) instrument (Justice at al.,

25 2002). The resulting reflectivity gradient associated to a particular reflectance pattern is assumed to provide an additional source of error if the footprints from on- and off-line laser pulses do not spot on the same target on ground (Ehret et al., 2008). Such footprint shifts may occur either from misalignment of the transmitted laser beams (e.g. laser pointing jitter) or from the finite time separation between the on-line and off-line

pulses. This separation is required to avoid the simultaneous presence of the two pulses in the lower part of the atmosphere, a situation which could lead to ambiguities in the returned signals. Due to the satellite velocity (close to 7000 m/s for low-altitude orbits), the time delay (typically larger than 200 microseconds) creates a spatial shift of
5 a few meters between the areas illuminated by the laser pulses on-ground.

To analyse the particular error contribution and to setup an optimum sensor design for the A-SCOPE mission a better data basis on the relevant surface reflectance as well as its variability in the spectral domain around 1.57 μm is of outmost interest. Airborne measurements are suited for such kind of investigation because of the similar viewing
10 geometry as provided by the space-borne counter part. The small footprint on ground of a few meters in diameter allows to investigate the reflectance statistics over complex terrain with high spatial resolution. For the footprint size of the space borne sensor, which is in the order of 100 m, representative values (e.g. mean and variance) can be obtained from up-scaling of the airborne measurements. The high flexibility of the
15 aircraft platform allows for remote measurements at almost all geophysical locations around the world. Particular in Europe, strong gradients in the surface reflectivity are expected over areas with heavy land use (large agriculture areas with patches of forest and meadows) and snow cover combined with vegetation and wooded terrain, whereas measurements in winter and summer time would enable to observe seasonal trends.
20 In this study we investigate the surface reflectance at 1.57 μm using an airborne platform covering different terrains in Central and Western Europe as well as the Baltic and Mediterranean Sea. The focus is on the small scale reflectance variations. Section 2 describes the calculation of the retrieval error and different laser footprint upscaling approaches to establish a connection to spaceborne systems. In Sect. 3 the experimental
25 setup and the measured data are described. Section 4 gives an overview of the collected data. In Sect. 5 the comparison of the collected data with absolute reflectances from satellite measurements is shown and a calibration using these data is discussed. Section 6 shows a comparison and discussion of the different upscaling approaches. Section 7 summarizes the results of statistical analyses. In Sect. 8 the retrieval error

Airborne lidar reflectance measurements

A. Amediek et al.

|◄ | ►|

◄ | ►

Back | Close

Full Screen / Esc

Printer-friendly Version

Interactive Discussion

simulation results for the A-SCOPE system configuration on the basis of the collected data are presented.

2 Theory

2.1 Calculation of the retrieval error

The retrieval error of a trace gas IPDA measurement introduced by ground reflectance variations is derived from the hard target lidar equation as shown in Ehret et al. (2008). The relative error of the trace gas column mixing ratio X_{gas}, if $\rho_{on} \neq \rho_{off}$, turns out to be

$$\frac{\delta X_{gas}}{X_{gas}} = \frac{1}{2\,\Delta\tau_{gas}} \ln \frac{\rho_{on}}{\rho_{off}} \tag{1}$$

with the lidar ground reflectances ρ for online and offline and the differential optical depth of the gas column $\Delta\tau_{gas}$. The logarithm can be approximated by its expansion in power series up to first order:

$$\ln \frac{\rho_{on}}{\rho_{off}} \approx \frac{\rho_{on} - \rho_{off}}{(\rho_{on} + \rho_{off})/2} \equiv \frac{\delta\rho}{\rho} \tag{2}$$

which corresponds to the relative difference of the reflectances, here named as $\delta\rho/\rho$.

2.2 Laser footprint up-scaling

The DLR airborne system TROPOLEX, used in this study, provides a high spatial resolution of the ground reflectivity composed of single footprints having a diameter below 10 m along the ground track of the aircraft with a footprint distance of about 10 m. In order to transfer the obtained lidar reflectance data to systems with larger footprints, the measurement data have to be up-scaled. Conceivable satellite systems using the IPDA technique will provide laser ground spot diameters on the order of several tens of

meters. Several approaches for an appropriate upscaling procedure are shown in the following. A comparison and a discussion are given in Sect. 6.

2.2.1   1-D up-scaling

The first method is what we call 1-D upscaling. To account for the larger beam size of a spaceborne IPDA instrument, the measured lidar reflectivity data are averaged. In principle the required averaging is 2 dimensional, but measurements are available only in one direction, the aircraft track. The 1-D up-scaling approach is calculated like a running average along the aircraft track. So the original resolution of the data is maintained. The up-scaled reflectivity ρ^{upsc} is calculated by:

$$\rho_i^{\text{upsc}} = \frac{1}{n} \sum_{j=i}^{i+n-1} \rho_j \tag{3}$$

with ρ as the measured lidar reflectivity, the number n of averaged measurement shots. The calculations shown here base on an assumed footprint diameter of a spaceborne instrument of about 100 m, i.e. $n=11$.

An alternative is to multiply an optional weighting function g to the reflectivity values within each "ground spot" interval to consider a beam intensity profile deviating from a top hat profile:

$$\rho_i^{\text{upsc,w}} = \frac{\sum_{j=i}^{i+n-1} g_j \, \rho_j}{\sum_{j=i}^{i+n-1} g_j} \tag{4}$$

Here, a gaussian weighting with a FWHM of 38 m was assumed.

The relative reflectivity difference $(\delta\rho/\rho)^{\text{upsc}}$ that is needed to yield the retrieval error is calculated accordingly to Eq. (2) using consecutive values ρ_i^{upsc} and ρ_{i+1}^{upsc} as online and offline.

2.2.2 Auto-correlation method

The Auto-correlation method is a more rigorous two-dimensional up-scaling method, but only allows access to limited information. It uses the auto-correlation of the reflectivities measured by TROPOLEX, which is calculated for a set of N data points with

$$C_{1-D}(x_i = i \cdot \delta x) = \frac{\sum_{j=1}^{N-100} \delta\rho_j \delta\rho_{j+i}}{\sum_{j=1}^{N-100} \delta\rho_j \delta\rho_j} \tag{5}$$

$$\delta\rho_j = \rho_j - \frac{1}{N}\sum_{k=1}^{N} \rho_k$$

$$0 \leq i \leq 100$$

δx is the spatial sampling distance between two successive measurements, and the value of 100 has been chosen as being large enough to provide information about C_{1-D} over the spatial scale of interest, while being an order of magnitude smaller than N. Provided a sufficiently large dataset is used, C_{1-D} is a smooth function, thanks to the averaging along the aircraft track involved in its calculation. The calculated auto-correlation function can be extended to two dimensions, using only the assumption of isotropy:

$$C_{2-D}(r_i = i \cdot \delta x, \varphi) = C_{1-D}(x_i = i \cdot \delta x) \tag{6}$$

The equivalent 2-D autocorrelation function $C_{2\,\mathrm{Davg}}(r_i, \varphi)$ that corresponds to the up-scaled reflectivities can be calculated from $C_{2-D}(r_i, \varphi)$ and, as will be shown, useful information about the statistics of the up-scaled reflectivities can be extracted from it. To present the principles behind its calculation, expressions involving continuous functions are used. The use of discrete valued functions would involve more complicated notations, but is equivalent. It is assumed that the reflectivity up-scaled to a

larger laser footprint $\rho_{2\,\text{Davg}}(x, y)$ can be expressed as the following integral involving the TROPOLEX reflectivity $\rho(x, y)$ and an averaging function $B(x, y)$ that describes the spatial distribution of laser light within the beam:

$$\rho_{2\,\text{Davg}}(x, y) = \int\int \rho(x_0, y_0)B(x_0 - x, y_0 - y)dx_0 dy_0 \tag{7}$$

$$\int\int B(x_0, y_0)dx_0 dy_0 = 1$$

$\delta\rho(x, y)$ and $\delta\rho_{2\,\text{Davg}}(x, y)$ denote the differences between the reflectivities $\rho(x, y)$ and $\rho_{2\,\text{Davg}}(x, y)$ and their mean values calculated by a spatial average into the full 2-D plane. Then

$$\delta\rho_{2\,\text{Davg}}(x, y) = \int\int \delta\rho(x_0, y_0)B(x_0 - x, y_0 - y)dx_0 dy_0 \tag{8}$$

This last result can be written

$$\delta\rho_{2\,\text{Davg}}(x, y) = \delta(x, y) * B(-x, -y) \tag{9}$$
$$\delta\rho_{2\,\text{Davg}}(-x, -y) = \delta(-x, -y) * B(x, y)$$

The autocorrelation function of the averaged reflectivity is

$$C_{2\,\text{Davg}}(x, y) = \int\int \delta\rho_{2\,\text{Davg}}(x_0, y_0)\delta_{2\,\text{Davg}}(x + x_0, y + y_0)dx_0 dy_0 \tag{10}$$
$$C_{2\,\text{Davg}}(x, y) = \delta_{2\,\text{Davg}}(-x, -y) * \delta\rho_{2\,\text{Davg}}(x, y)$$
$$C_{2\,\text{Davg}}(x, y) = [\delta\rho(-x, -y) * \delta\rho(x, y)] * [B(-x, -y) * B(x, y)]$$

$$C_{2\,\text{Davg}}(x, y) = C_{2D}(x, y) * [B(-x, -y) * B(x, y)] \tag{11}$$

Airborne lidar reflectance measurements

A. Amediek et al.

All the information to calculate $C_{2\,Davg}$ is available. The averaging function B is usually analytical (a circular hat and a Gaussian will be considered in our work) so that $B*B$ can be calculated analytically. Thus, only one 2-D numerical convolution is required. The variance $\text{Var}(\Delta\rho_{2\,Davg}, i)$ of the reflectivity change between two points separated by the distance $i \cdot \delta x$ can be obtained from $C_{2\,Davg}$ as follows

$$\text{Var}(\Delta\rho_{2\,Davg}, i) = \frac{1}{M} \sum_{j=1}^{M} (\rho_{2\,Davg,j+i} - \rho_{2\,Davg,j})^2 \tag{12}$$

$$\text{Var}(\Delta\rho_{2\,Davg}, i) = \frac{1}{M} \sum_{j=1}^{M} \left[\delta\rho_{2\,Davg,j+i}^2 + \delta\rho_{2\,Davg,j}^2 - 2\delta\rho_{2\,Davg,j}\delta\rho_{2\,Davg,j+i} \right]$$

$$\text{Var}(\Delta\rho_{2\,Davg}, i) = 2\text{Var}(\rho_{2\,Davg})[1 - C_{2\,Davg}(i \cdot \delta x)]$$

It is possible to include in the procedure a deconvolution of the measurements from the initial TROPOLEX beam shape. In the paper this additional step is not considered.

2.2.3 Up-scaling method for sea surfaces

The sea surfaces measured by TROPOLEX were found to have a very short correlation length, clearly smaller than the measurement sampling distance (see Sect. 7.2). In this context, a model will now be built to describe the up-scaling of un-correlated reflectivities. It aims to improve the reliability of the up-scaling procedure and to get a better understanding of the measurements. First, it is assumed that the correlation length of the lidar reflectivity is much smaller than any distance considered in our treatment. For convenience, we will formally define a lidar reflectivity $\rho(x, y)$ at every location (x, y), being fully uncorrelated in the spatial dimensions. This reflectivity function, once averaged within the footprint where the spatial distribution of laser light is $B(x, y)$, becomes

$$\rho_{B,i} = \frac{\int\int \rho(x, y)B(x - x_i, y)dxdy}{\int\int B(x, y)dx\,dy} \tag{13}$$

Using the property $\text{Var}[\int\int \rho(x,y)dx\,dy] = kS$ on very small areas S where $B(x,y)$ is nearly constant, the variance of $\rho_{B,i}$ can be calculated

$$\text{Var}(\rho_{B,i}) = \frac{\text{Var}\left[\int\int \rho(x,y)B(x-x_i,y)dx\,dy\right]}{(\int\int B(x,y)dx\,dy)^2} = k\frac{\int\int B^2(x-x_i,y)dx\,dy}{(\int\int B(x,y)dx\,dy)^2} \tag{14}$$

$\text{Var}(\rho_{B,i})$ is now evaluated in two cases. For a top hat circular footprint, it is simply inversely proportional to the area S. The up-scaling of the variance from the TROPOLEX beam with area S_0 to a larger beam with area S_1 is

$$\text{Var}(\rho_{S_1,i}) = \text{Var}(\rho_{S_0})\frac{S_0}{S_1} \tag{15}$$

For a Gaussian beam the variance is

$$B(x,y) = \frac{1}{2\pi\sigma^2}\exp\left(-\frac{x^2+y^2}{2\sigma^2}\right) \tag{16}$$

$$\text{Var}(\rho_{B,i}) = \frac{k}{4\pi\sigma^2}$$

The up-scaling from a TROPOLEX Gaussian beam with σ_0 to a space borne lidar with σ_1 is given by

$$\text{Var}(\rho_{B_1,i}) = \text{Var}(\rho_{B_0,i})\frac{\sigma_0^2}{\sigma_1^2} \tag{17}$$

Now the variance of the difference between $\rho_{B,i}$ evaluated at two different points (denoted by i and j) is calculated, as the function of the separation distance L between the two footprints. Depending on the value of L, there can be some overlap between the two footprints and the result needs to account for this possibility.

Airborne lidar reflectance measurements

A. Amediek et al.

Full Screen / Esc

Printer-friendly Version

Interactive Discussion

$$\text{Var}[\Delta\rho(L)] = \text{Var}[\rho_{B,j} - \rho_{B,i}] \tag{18}$$

$$= \text{Var}\left(\frac{\int\int \rho(x,y)[B(x-L-x_i,y) - B(x-x_i,y)]dx\,dy}{\int\int B(x,y)dx\,dy}\right)$$

$$= k\frac{\int\int[B(x-L,y) - B(x,y)dx\,dy]^2}{\left(\int\int B(x,y)dx\,dy\right)^2}$$

For a top hat circular footprint with radius R_1 and area S_1 the expressions simplify. They explicitly include the fraction $O(L)$ of the area S_1 that overlaps with the second footprint, defined such that $O(0)=1$ and $O(2R_1)=0$.

$$O(L) = \begin{cases} \frac{2}{\pi}\arccos\left(\frac{L}{2R_1}\right) - \frac{L}{\pi R_1^2}\sqrt{R_1^2 - \frac{L^2}{4}} & \text{if } L \le 2R_1 \\ 0 & \text{if } L \ge 2R_1 \end{cases} \tag{19}$$

$$\text{Var}[\Delta\rho(l)] = 2\text{Var}(\rho_{S_1,i})[1 - O(L)] \tag{20}$$

For a Gaussian footprint defined with parameter σ_1 we find

$$\text{Var}[\Delta\rho(L)] = 2\text{Var}(\rho_{B_1,i})\left[1 - \exp\left(-\frac{L^2}{4\sigma_1^2}\right)\right] \tag{21}$$

These two expressions, applicable for the uncorrelated reflectivities observed over sea, have a similar structure as the results obtained in Sect. 2.2.2 with the auto-correlation method.

3 Experimental setup

3.1 Instrument

The lidar system employed in this study is the DLR's TROPOLEX system (Meister et al., 2003), which is designed for use on board the DLR research aircraft Cessna Grand Caravan 208B (D-FDLR) as shown in Fig. 1. It consists of a laser system, a down-looking receiving unit and a data acquisition unit. Some modifications of the original system which was designed for the measurement of tropospheric ozone were necessary for this study. The modified system provides 5 mJ per pulse at 1.573 μm wavelength with a 10 Hz repetition rate. The output power is monitored for the relative calibration of the outgoing pulses. Table 1 summarizes the main parameters of the system.

Figure 2 shows the layout of the system. It operates in bistatic configuration, with a laser transmitter and a separate receiving telescope. A flashlamp pumped Nd:YAG laser operating at its fundamental frequency (1.064 μm) is used to pump an optical parametric oscillator (OPO) (Giordmaine and Miller, 1965; Tang et al., 1992) with a KTP-crystal as the non-linear medium (size: $5 \times 5 \times 20$ mm^3). The OPO converts the 1.064 μm-radiation into 1.573 μm (signal) and 3.3 μm (idler). The idler radiation is not used here. A small part of the signal radiation is picked up and guided to an integrating (Ulbricht) sphere, where an InGaAs-PIN-diode is installed for the power reference measurement of each laser pulse. The outgoing beam diameter is about 1 cm and adjusted to a beam divergence of 3 mrad. The beam is guided downwards out of the aircraft. There is a constant off-nadir angle of about 1.2° to the forward direction in addition to temporally occurring roll and pitch angle variations of the aircraft. A down-looking Cassegrain type telescope (4 mrad field of view) collects the light backscattered by the ground. Then it is focused on a diffusor and imaged onto the detector. This diffusor considerably enhances the signal stability. A second InGaAs PIN diode (1 mm diameter of the active area) serves as the detector. A polarisation filter can be inserted into the receiver light path and removed during the measurements (transmission 98%, contrast

>10 000:1). It is adjusted orthogonally to the outgoing laser beam polarisation. So the depolarized part of the backscattered light can be detected. Here, the filter was only used in some selected cases (see Sect. 7.3). The major part of the measurements was performed without the filter.

5   Additionally, there are two cameras installed for monitoring the ground area around the telescope's field of view: one operating in the visible spectrum and another one in the near IR, limited by a bandpass filter to the range between 1500 nm and 1600 nm. The captured pictures are used to identify the ground surface types.

The employed Cessna Grand Caravan 208B is an one engine turboprop aircraft that
10 provides special apertures at the bottom side of its body for the use of down-looking scientific instruments. It provides a non-stop range of more than 1000 km and can be used for overflights of the sea up to 10 km offshore. The flight altitude above ground during the measurements was between 1.5 and 3 km, the ground speed was between 290 km/h and 360 km/h.

15 **3.2   Measured data**

The collected raw data contain the output-power monitor data, the ground reflex data and the distance to the ground calculated from the laser pulse runtime. Due to the high temporal bandwidth of the detector/preamplifier system of 4 MHz spatially structured targets, such as trees, cause temporally structured return signals. To compensate for
20 this effect, lidar reflectivity data are calculated by integrating the whole pulse return that is detected in the detector sampled signal.

The ground reflex data are normalized by the corresponding output-power data. Additionally, the ground reflex data are corrected with respect to ground distance variations that occur due to the orography and aircraft altitude changes. The resulting
25 quantity (named as ρ, in arbitrary units) is assumed to be proportional to the absolute lidar ground reflectance ρ^* (in sr^{-1}). Additionally the data are geo-referenced using an on-board differential GPS system. Furthermore, data about the aircraft attitude are available.

Airborne lidar reflectance measurements

A. Amediek et al.

The spectral bandwidth of the generated OPO radiation is 0.2 nm. This is much broader than the absorption lines of water vapor and carbon dioxide that occur in this wavelength region and so there is no significant absorption. Numerical simulations showed, that absorption changes due to variations of the CO_2 and H_2O concentra-
5 tions or of the flight altitude as well as possible wavelength instabilities do not have a noticeable influence on the ground reflectivity measurement.

The beam attenuation due to atmospheric aerosol scattering and absorption was not corrected, since the main focus of this investigation was on the relative reflectivity variability on the order of several tens of meters, on which no significant changes of the
10 aerosol load is expected.

The typical laser footprint diameter on ground is 5 m to 9 m depending on the distance from the aircraft to the ground. The center-to-center distance between two consecutive footprints is between 8 m and 10 m, depending on the aircraft ground speed. So normally there is no overlap and an almost continuous capture of the ground reflec-
15 tivity with a high spatial resolution is achieved.

An analysis of the TROPOLEX's instrumental noise was performed by means of a reference measurement in the laboratory using a stationary and defined target with a flat and homogeneous surface: a wall made of construction concrete in 100 m distance to the system. Due to the comparable short distance to the target possible atmospheric
20 influences are not considered here. So, only the instrumental noise appears. Table 2 shows the results for all quantities that are derived from the measurement data (the definitions are given in the respective sections). The given values are calculated using the same routines that are used for the data analysis. The values of the absolute reflectance precision base on a calibration using ASTER spectral library data (Baldridge
25 et al., 2009). Since the detector/preamplifier noise is well below the obtained values, it is assumed that the noise is mainly caused by electromagnetic interference due to the high voltages of the laser's q-switch and by an imperfect power reference measurement which turned out to be critical in previous measurements (Amediek et al., 2008).

4 Measurements

The measurement flights performed during this project provide data covering more than 5000 km ground track length (see Fig. 3). From these data, 25 flight legs have been extracted with individual lengths between 30 and 340 km, and an overall length of
5 more than 3300 km, each providing continuous data without interruptions due to cloud coverage or other reasons. Several local flights during different seasons took place in the alpine upland close to Oberpfaffenhofen airfield (Southern Germany). Long range flights to the Baltic Sea across Germany and to Spain via France and Portugal yield data from different regions with various terrains. Flights over the Baltic Sea as well as
10 the Mediterranean Sea offer data about the sea surface reflectivity.

The flights took place in December 2007, April and June 2008. They cover grass-lands, forests, different agricultural landscapes, lakes, the open sea, partly snow cov-ered terrains, mountainous and rocky areas, very dry regions with sparse vegetation and urban areas. Most types of arid and humid regions occurring in Central and West-
15 ern Europe were captured.

The Figs. 4 and 5 show typical measurement results collected during the flight mis-sions. In the upper part of each plot the aircraft to ground distance is depicted, the middle part shows the non-averaged reflectivity (10 m horizontal resolution) and at the bottom a kind of quality flag indicates filtered single values (a vertical peak upwards in
20 the case of detector overload or clouds, downwards in the case of a very weak signal). A second y-axis on the left side indicates absolute reflectances ρ^*, obtained by using MODIS data along the respective flight tracks (see also Sect. 5).

The plots a) and b) of Fig. 4 show two measurements of the same 50 km track, performed in April and June, as demonstrated by the ground distance curve showing
25 an identical orography signature. These data show the same terrain during different seasons: before the vegetation period with patches of old snow in April, and at the beginning of the vegetation period in June. The reflectivity measured in April is signifi-cantly decreased in the middle part of the leg, where the snow patches occurred.

Airborne lidar reflectance measurements

A. Amediek et al.

The flight across Germany to the Baltic sea (April) is plotted in c) (Southern Germany) and d) (Northern Germany) of Fig. 4. At kilometer 275 in plot d) the coast was crossed to the open sea. The landscape in Southern Germany is dominated by small structures (farmland, forest, populated areas), while Northern Germany shows more large scale structures (less forests, more and larger agricultural fields).

Figure 5 displays flight legs in Spain (a–c) and Southern France (d) measured in June. In general the ground surface in Spain is dryer than in France and Germany. Plot a) in South-West Spain represents an area, that is dominated by agricultural fields and forests. Plot b) depicts a 630-km flight leg with different surface types in Southern Spain: large olive groves at the beginning, the mountains of the Sierra Nevada, then a very arid section, the Mediterranean Sea, a section with inland water bodies (Mar Menor close to Murcia, known for its smooth surface) alternating with land and several crossings of the costal line, and at the end again mountainous terrain and partly farmed ground (see also Fig. 7). Plot c) shows a flight leg over the Mediterranean Sea and plot d) a region in Southern France dominated by agricultural land and forests.

Figure 6 shows a 9-km-zoom into the flight performed in April 2008 (Southern Germany) to give an impression of the small scale reflectance variability. This example contains snow covered grassland sections, a small settlement and forests that have parts sparsely covered with trees. The lower panel depicts the relative reflectivity differences $\delta\rho/\rho$.

5 Absolute reflectances using MODIS and Cox and Munk

5.1 Comparison to MODIS data

The TROPOLEX system itself is not able to provide absolute lidar reflectance data, but a calibration by means of external data can be performed, for example using satellite data from passive sensors. The connection between the data sets can be done by using the geo-location information. Here, the collected data are compared to band

6 data of the Moderate Resolution Spectroradiometer (MODIS) on board the Terra and Aqua satellites which provides land surface reflectance data in the spectral range between 1628 nm and 1652 nm, thus close to the TROPOLEX wavelength. Here, the data product MOD09A1 (level-3, 8-day composites, 500 m spatial resolution, aerosol corrected) was used (Justice at al., 2002).

After the connection of the data it is possible to access to absolute reflectance values at the TROPOLEX's spatial resolution of 10 m, thus far below the resolution of MODIS. Furthermore the lidar reflectance of the sea surface can be determined, which is not provided by MODIS.

The performed procedure can be seen in Fig. 7. It shows again the 630-km flight leg between Cordoba and Valencia in Southern Spain. Here, both TROPOLEX and MODIS data are plotted for the same ground track. The TROPOLEX data are averaged along 500 m to get a spatial resolution closer to the MODIS data. The scale of the MODIS reflectance data is adapted in a way, that the best possible matching is achieved for the whole flight. Then, one calibration factor is determined for each continuous measurement flight. In general, the agreement of the data is very good, but it has to be mentioned, that the comparability of the different data is not automatically given. One point is, that a (500×500) m^2 MODIS pixel is compared to the narrow TROPOLEX ground track. So dependent on the respective surface structure a certain deviation is expected. Another aspect are the different wavelength regions, which cause higher MODIS values, between 1.5% and 15%, compared to TROPOLEX measurements depending on the surface type (according to ASTER). Furthermore the lidar configuration always measures the "hot spot" (view angle is equal to the light incident angle) (Hapke et al., 1996; Bréon et al., 2002), whereas the used MODIS product does not consider this effect. For some surface types this could lead to higher TROPOLEX values. Changes of the aerosol load of the atmosphere within a flight leg could also lead to deviations. A validation of the MODIS data is performed by Liang et al. (2002). In their test measurements they found an error of less than 5%. Due to the unknown contributions of the mentioned points no corrections were made at this stage of the

Airborne lidar reflectance measurements

A. Amediek et al.

data analysis.

5.2   Land and sea surfaces reflectances

In the next step, those land surface types were identified that show the minimum and maximum reflectances. Snow covered grassland areas (observed in Southern Germany) are identified to show the lowest reflectance of all solid surfaces: ρ^*=0.012 sr^{-1} (average value). The highest reflectance was found in Southern Spain and identified as dry grass (in olive groves): ρ^*=0.18 sr^{-1} (average value). Single measurement points can exceed these limits considerably as shown in the discussion about the dynamic range below.

A spot-checking of calibrated reflectances of some identified surface types indicates a good accordance to the data of the ASTER spectral library (e.g. for the above mentioned snow and dry grass areas). Reflectance changes within a flight leg, also on small spatial scales, are mostly reproduced with good accordance between TROPOLEX and MODIS, as can be seen in Fig. 8.

One important result of this study is the fact, that on average the observed sea surface reflectivity level is almost one half of the level that is obtained over land. Noticeable differences in the sea reflectance level during a flight often could be correlated with observable differences of the sea surface structure (recorded by the vis-spectrum-camera).

All flight legs that contain sea overflights can be calibrated using the land surface information within the same flight to get the absolute reflectance by means of MODIS data. In this way a reflectance of the sea surface between 0.02 sr^{-1} and 0.05 sr^{-1} was derived (on the basis of 1-km averages to smooth the small scale variations). The wind speeds during the corresponding measurements were quite low, between 2 m/s and 5 m/s without whitecaps.

5.3 Comparison to Cox and Munk

A noticeable discrepancy occurs, if the sea surface reflectances, obtained by the procedure shown above, are compared to the expected reflectances calculated on the basis of Cox and Munk (1954). Here, values between $0.045\,\mathrm{sr}^{-1}$ and $0.125\,\mathrm{sr}^{-1}$ result for the conditions that were existent during the measurements (wind speed and off-nadir angles between 1° and 5° due to the aircraft attitude). That would indicate an under-estimation of the MODIS calibrated measurements, if it is performed as described above, by a factor of up to 2. Camacho-de Coca et al. (2004) investigated the mentioned hot spot effect for different agricultural crops in the spectral range between 440 and 2200 nm by airborne measurements. They observed at 1593 nm a hot-spot reflectance enhancement factor around 1.6 for Alfalfa and Barley. Kaasalainen et al. (2006) investigated the hot spot peak properties for snow and lichens (Kaasalainen and Rauiainen, 2005). So, this effect could be an explanation of the discrepancy for the most part, which would mean, that the used MODIS data under-estimate the lidar reflectance of the ground.

6 Comparison of the different upscaling approaches

A special flight was performed during this project to compare the various up-scaling methods with real data in a case study. The flight pattern was arranged in a way, that the same 50-km route was flown 8 times very precisely using the aircraft Navigation System. Hereby, the single tracks have a distance of about 10 m to 20 m to each other, spaced orthogonally to the flight direction. So, by means of the geo-location information of the data a 2-D reflectivity array, with about 100 m in width, was obtained that allows the composition of larger footprints. The flight took place in April 2008 in the alpine upland in Southern Germany. The region is dominated by alternatingly occurring small forests, grassland and settlements. Due to the landscape characteristic and the fact that there were patches of old snow the reflectance variability was relatively high.

The up-scaling to 100-m 2-D footprints is done as follows. Each single footprint is composed by cutting out a square from the data array (about 80 single measurements). Then, the data within such a square are weighted with a two-dimensional gaussian function with 38 m FWHM. This method allows to simulate the real footprint of a space borne laser system. The next footprint is calculated accordingly by using the array shifted by one row (10 m).

Figure 9 shows a comparison of the different up-scaling approaches on the basis of this 50-km test route. The 1-D approaches use the information from the mid-track of the 2-D array. The plots depict the reflectivity differences depending on a variable spatial gap between two ground spots along the track. The resulting curves for the 1-D upscaled data (using un-weighted reflectivities ρ, according to Eq. (3), as well as Gaussian weighted, according to Eq. 4) and for the 2-D data (only Gaussian weighted) are calculated as follows

$$\Delta\rho_{j,i} = (\rho_j - \rho_{j+i}) \tag{22}$$

where the gap is represented by $i \cdot \delta x$ (for $\delta x \approx 10$ m). For each i corresponding to gaps between 0 and 350 m the resulting RMS values of $\Delta\rho(i)$ are plotted on the basis of all measurements j along the 50-km-track section. The results of the autocorrelation method are calculated using Eq. (12).

In general one would expect, that the reflectivity differences calculated from 1-D up-scaled data are overestimated noticeably compared to results from real 2-D footprints, since one can assume, that the averaging of the small scale differences using two dimensions causes a stronger smoothing. On the other hand consecutive reflectivity values show a correlation on short scales as shown in Sect. 7.2. So, the overestimation of the 1-D averaged reflectivities is not as strong as should be expected for uncorrelated data. The plots indicate that the 1-D upscaling overestimates the reflectivity differences compared to the 2-D data as expected. The gaussian-weighted 1-D upscaling is too pessimistic, whereas the un-weighted 1-D upscaling is more realistic. In general the weighting enhances the contribution of the footprint center. This is equivalent to a decrease in the footprint size. As a result the averaging efficiency decreases.

Airborne lidar reflectance measurements

A. Amediek et al.

|◄ | ►|

◄ | ►

Back | Close

Full Screen / Esc

Printer-friendly Version

Interactive Discussion

The results from the autocorrelation approach are close to the 2-D results. The un-weighted case under-estimates the reflectance differences, as expected, and so it should not be used. The weighted case is expected to give the most accurate estimate of the real 2-D footprints. Its only assumptions are: isotropy and stationarity of the reflectance statistical properties. According to Fig. 9, there is however a slight discrepancy between the auto-correlation approach with unweighted measurements and the real 2-D footprints. This could be explained by the observed fact, that the measured reflectivity increased slightly during the execution of the 2-D flight pattern, probably due to a drying of the surface in the morning.

The un-weighted 1-D upscaling turns out to be an acceptable representative for gaussian-weighted 2-D footprint. It is easy to calculate and the continuous data stream allows an access to single selected data along the flight track. The remaining overestimation of the reflectivity differences involve, that the derived retrieval errors can be treated safely as upper bounds. All results given in the following sections that refer to upscaled data base on the un-weighted 1-D upscaling.

7 Characteristics of lidar ground reflectivity

7.1 Dynamic of the reflectivity

An important point for the design of a measurement system is the occurring signal dynamic which is in case of IPDA strongly dependent on the ground reflectances. The measurement sensitivity of the instrument should fulfill the requirements for all occurring ground reflectances as far as possible. Since Earth's ground albedo is highly variable in the visible spectrum, the lidar reflectance in the IR-range is suspected of being variable in the same manner, which is already indicated by the ground reflectance data of the ASTER spectral library (Baldridge et al., 2009) or MODIS (Justice at al., 2002).

The measurement data (see Figs. 4 and 5) confirm this assumption. Regarding all flights of this project, as the maximum contrast between the darkest and the brightest

solid surface a factor of 15 was found for snow covered grassland in Southern Germany $(0.012\,\mathrm{sr}^{-1})$ compared with dry grass in Spain $(0.18\,\mathrm{sr}^{-1})$. If one looks onto the reflectivities of all single extracted flight legs, it results, that the corresponding RMS values for different landscapes vary between 21% and 38%, if no snow coverage occurred. Flight legs with partly snow covered ground in a region with a complex spatial structure on a small scale, like in Southern Germany (forests, grassland, agricultural fields, populated areas), showed the highest reflectivity dynamic with RMS values up to 90%. Figure 10 gives typical examples of the reflectivity distribution for different surface types. The plots shown in Fig. 11 base on the same data and depict the occurence of the absolute reflectance differences $\delta\rho^*$ dependent on the respective absolute reflectance.

Another detail that is indicated by the measurements is the occurrence of single reflectivity extrema, which could exceed the surrounding reflectivity level considerably up to the detection limit of the system. By means of the down-looking cameras most of the surface types that come along with these cases could be identified. They occur cumulatively in urban areas, where a factor of up to 5 was typical for single extrema. Lakes and rivers can cause stronger outliers, resulting in both very weak as well as very high values, mostly alternating on a short spatial scale.

In addition to the reflectivity dynamic, the reflectivity changes on small scales must also be characterized since they can cause an IPDA retrieval error. This aspect is treated in the following.

7.2 Small scale reflectivity changes

Due to the high spatial resolution of the measurements a quantification of the reflectivity changes on short scales which could affect the IPDA measurement can be performed.

Figure 12 depicts the auto-correlation of the reflectivity (non-upscaled) for four exemplary flight legs with three different land use types and the open sea. The signal from the sea turns out to be totally uncorrelated, while the signals from the land surfaces show correlations with different grades. The figure confirms the expected connection between the apparent spatial structure of the land use type and the correlation length

by trend. Nevertheless a classification is not possible, since the auto-correlation functions vary strongly, also for apparently similar surfaces. Figure 9 showed the behavior of the reflectivity differences depending on the spot separation distance. The non-linear increase is determined by the overlap of the ground spots (here up-scaled) and by the correlation of the reflectivity along the track. The best description of the curve shapes was obtained with exponential fits. Due to the non-linear characteristic a reflectivity gradient that allows a direct transfer to different spot separating distances is only possible for very short separating distances.

An example for the distribution of the reflectivity differences $(\delta\rho/\rho)_{10m}$ (for 10 m spatial distance) is depicted in Fig. 13, calculated according to Eq. (2). Due to the isotropy of the ground surface structures the distribution is almost symmetrical with respect to zero. The mean reflectivity difference of the shown case (50 km flight leg, high variability due to partial snow coverage, about 6500 measurements) is 0.4%. Along with footprint up-scaling the RMS of $(\delta\rho/\rho)_{10\,m}$ reduces noticeably from 29.9% to 4.4%. Table 3 summarizes the minimum and maximum values for $(\delta\rho/\rho)_{10\,m}$, regarding all available flight data, each represented by RMS values on the basis of 50-km-sections.

The comparison of the same 50-km-ground track during different seasons showed a considerable increase of the $(\delta\rho/\rho)_{10\,m}$ for the April-flight (with partial snow coverage) in comparison to the June-flight – in this particular case: 18% (June) and 30% (April) with respect to the original data; 2.5% (June) and 4.5% (April) with respect to the up-scaled data.

The RMS of the reflectivity from flight legs over the sea varies between 12% and 27%. So, in general the variability (absolute as well as relative) was lower than over land surfaces. For sea surfaces the RMS of the reflectivity differences $(\delta\rho/\rho)_{10\,m}$ for up-scaled laser footprints (100 m) turned out to be small, between 0.36% and 0.82% (using Eq. 20).

Airborne lidar reflectance measurements

A. Amediek et al.

7.3 Observation of polarization effects

The application of the polarization filter in the receiving path that allows the measurement of the depolarized part of the backscattered laser light led to the following observations. The occurrence of the above mentioned high signal extrema was reduced considerably. So one can conclude that the high reflectivity cases often come along with non-depolarizing backscatter, e.g. due to a specular character of the corresponding surfaces. Nevertheless, the use of the polarisation filter did not show any significant effects on the characteristics of $\delta\rho/\rho$, as indicated by the direct comparison of a special flight leg that was exactly flown twice, with and without the filter.

Furthermore no depolarization of the received light from the sea surface could be detected, as expected. Special flight manoeuvres, in which the aircraft's roll angle was varied, showed the expected dependency of the signal strength on the off-nadir angle (Bréon and Henriot, 2006). At a certain angle the signal completely dropped down to zero. Both facts confirm, that at this wavelength the received signal is dominated by specular surface reflection and there is no sub-surface backscattering within the range of the measurement sensitivity.

For land surfaces the signal amplitude, when using the polarization filter, was about one third compared to the signal without the filter (between 29% and 37%). A full depolarization of the polarized laser light by surface backscattering would lead to a signal amplitude of almost 50%. That indicates that the ground surface backscattering does not completely depolarize the laser light, which also was observed for example for corn fields by Kalshoven et al. (1995) and for clover by Woessner and Hapke (1987). Differences in the amount of depolarization could not be correlated to the surface type on the basis of the available data.

Airborne lidar reflectance measurements

A. Amediek et al.

Title Page

Abstract | Introduction

Conclusions | References

Tables | Figures

◄ | ►

◄ | ►

Back | Close

Full Screen / Esc

Printer-friendly Version

Interactive Discussion

8 Simulation of a satellite instrument

One of the main goals of this study was to use the obtained lidar ground reflectance data to derive the retrieval error that would be introduced in a spaceborne IPDA measurement by an imperfect online/offline-overlap using the example of A-SCOPE. The configuration parameters used are summarized in Table 4.

The A-SCOPE laser footprint is assumed to have a gaussian beam intensity distribution, with a full width half maximum of 38 m on ground. More than 99% of the incident energy is enclosed in a circular footprint with a diameter of 100 m on ground. To upscale the reflectivity data to this footprint, the 1-D unweighted up-scaling method is used with an averaging interval of 100 m length. As already mentioned, this method is very simple to implement and gives an estimate of the real 2-D gaussian averaging.

The A-SCOPE instrument will average the obtained data over a 50 km path length to decrease the statistical noise. Due to the 50-Hz laser double pulse repetition rate, a number of about 350 averaged measurements results. To account for this measurement strategy, the calculation of the retrieval error generated by an imperfect overlap using the TROPOLEX data is also based on 350 measurements selected from 50-km ground track intervals, using the same spatial sampling as for A-SCOPE. The simulation principle is described by Fig. 14. The analogy to the conditions of A-SCOPE measurements gives a realistic impression about the distribution of occurring retrieval errors from real ground tracks. It emerged, that the retrieval error of a single 50-km interval depends strongly on the effectively selected data, so it depends strongly on the starting point within the interval. The whole dataset collected during this project contains 38 of such 50-km intervals from different regions across Europe (land surfaces), each providing a continuous ground track data stream without interruptions.

The retrieval error of the carbon dioxide column mixing ratio for a single 50-km-interval is calculated on the basis of the Eqs. (1), (2) and (3):

$$\delta X\text{CO}_2 = \frac{1}{2\,\Delta\tau_{\text{CO}_2}\,\left[\frac{\delta\rho}{\rho}\right]_{50\,\text{km}}} \cdot X\text{CO}_2 \tag{23}$$

with $[\delta\rho/\rho]_{50\,km}$ as the arithmetic mean of the 350 selected 1-D upscaled $(\delta\rho/\rho)$-values along the 50-km track section (100 m footprint, i.e. n=11, see Eq. 3), $\Delta\tau_{CO_2}$ as the differential optical depth of the CO_2 column and XCO_2 as the column mixing ratio of carbon dioxide. For the calculation of $\delta\rho/\rho$ the original shift of about 10 m

5 of the TROPOLEX data is taken. Hence, no further inter- or extrapolations of the collected data are done for the calculation of the resulting retrieval error. The expected online/offline overlap mismatch of a spaceborne system, such as A-SCOPE, is on the order of a few meters. So, 10 m is a pessimistic approach. The dominant contributor is the laser pointing jitter that can lead to shifts on ground up to 1/10 of the ground spot

10 diameter (as a worst case). The second factor is the platform velocity that causes a shift of about 1.5 m on ground assuming the A-SCOPE configuration. A minor reason is given by the satellite platform jitter due to micro-vibrations that can not be corrected by the attitude and orbit control systems (AOCS) of a satellite, which could cause a shift of about 0.5 m (ESA, personal communication, 2009).

15 However, the 50-Hz-pattern disregards many TROPOLEX data between consecutive A-SCOPE measurements: data are taken every 144 m, i.e. every 16 TROPOLEX measurements. To fully utilize the available dataset and to consider the dependence on the starting point, the pattern is shifted 15 times within each 50-km-interval, each by one TROPOLEX measurement. The original measurements are used several times by

20 this procedure, but the high spread of the results legitimates the use as independent values. So there is an ensemble of 16 retrieval error values for each 50-km-interval, which could be interpreted as 16 different satellite overflights along the same ground track.

Figure 15 shows a histogram of all calculated $[\delta\rho/\rho]_{50\,km}$ in percent and the resulting

25 retrieval errors in ppm (38 times 16 values are represented).

The RMS of all these single results is: $RMS[\delta\rho/\rho]_{50\,km}$=0.11% corresponding to δXCO_2=0.22 ppm. It has to be reminded, that these numbers base on conservative assumptions (1-D-upscaling procedure and large online/offline-mismatch) and so they are upper bounds. The retrieval error resulting for sea surfaces is below 0.1 ppm (cal-

culated on the basis of Eq. 20).

The precision requirements defined for A-SCOPE are below 1 ppm (ESA, 2008). So it results, that the contribution of the retrieval errors, introduced by the earth's surface reflectance variability, to the total instrument error budget is not negligible, but still in an acceptable range. Inversely, the requirements that have to be satisfied by the satellite system with respect to the online/offline ground spot overlap mismatch turn out to be around 10 m or below.

9 Summary and outlook

The IPDA lidar technique is a promising approach for measuring atmospheric CO_2, and has been proposed for the A-SCOPE ESA mission. The purpose of this study was to investigate the impact of ground lidar reflectivity variations which are creating radiometric errors specific to IPDA lidar systems. To do so, airborne measurements of the lidar ground reflectivity at 1.57 μm were performed with a high spatial resolution of about 10 m. The measurement flights performed cover regions in Central and Western Europe with typical terrains, both in semi-arid und humid regions: primarily agricultural land, forests, populated areas, mountainous regions and the open sea. Differential absorption lidars that use the ground reflex of a laser pulse are affected by the variability of the ground surface, if adjacent online and offline pulses hit different areas on ground. Due to the laser pointing jitter and the platform velocity of a spaceborne system, a difference in the geometrical overlap of the temporally separated online and offline measurements up to 10 m has to be expected.

The performed measurements showed, that the ground surface reflectivity is highly variable in the considered spectral region. On a scale of 10 m large reflectivity differences on the order of several tens of percent (RMS) occur from footprint to footprint, if footprint diameters on the same order are provided as basis. However, if larger footprints are of interest the reflectivity differences decrease noticeably. Conceivable satellite systems would have a laser footprint on ground with several tens of meters

Airborne lidar reflectance measurements

A. Amediek et al.

in diameter. Different approaches of upscaling the available data to larger footprints are investigated including a comparison to 2-D data, that are obtained by a special flight pattern. It results, that a simple 1-D averaging along a certain flight path interval leads to an acceptable approximation of a 2-D footprint with gaussian shape having a corresponding diameter. One characteristic of the reflectivity differences is their symmetrical distribution with respect to zero, which is expected due to the isotropy of the surface structures. Relevant is the number of measurements that have to be averaged to get acceptable values. Calculations using the available data showed, that for an assumed 100-m footprint diameter the averaging of 350 measurements along the track leads to a reduction of the reflectivity differences per 10 m to the order of 0.1%, which is compatible with a spaceborne IPDA error budget, such as assumed for A-SCOPE.

A first approach of an absolute calibration of the collected measurements using MODIS ground reflectance data was performed. Snow covered grassland was identified as the surface type showing the lowest reflectance ($0.012\,\mathrm{sr}^{-1}$) and dry grass occurring in Southern Spain as the surface with the highest reflectance ($0.18\,\mathrm{sr}^{-1}$). By means of the MODIS land surface data also access to the sea surface reflectance was given. For wind speeds between 2 and 5 m/s we deduced a reflectance between $0.02\,\mathrm{sr}^{-1}$ and $0.05\,\mathrm{sr}^{-1}$. However, according to Cox and Munk values between $0.045\,\mathrm{sr}^{-1}$ and $0.125\,\mathrm{sr}^{-1}$ were expected for the observed cases. The under-estimation of the lidar ground reflectance, if MODIS data are used for a calibration, could be explained by the hot-spot effect that is occurring in lidar measurements.

Some ground types that occur on Earth's surface are not captured in the framework of this project. Future measurements should focus on further ground types that cover large areas of the Earth, such as deserts, large snow covered areas with different snow types (Larsson et al., 2006), other types of forests (e.g. in the tropics), savannas, marshlands, tundra and sea surfaces under high wind speed conditions. Another issue that could have an impact on the surface reflectance is the surface humidity due to dew or just after rainfall (Twomey et al., 1986). In summary, the TROPOLEX system onboard the Cessna Caravan aircraft turned out to be an excellent tool to investigate

Title Page

Abstract | Introduction

Conclusions | References

Tables | Figures

◄ | ►

◄ | ►

Back | Close

Full Screen / Esc

Printer-friendly Version

Interactive Discussion

the ground surface variability.

References

Amediek, A., Fix, A., Wirth, M., and Ehret, G.: Development of an OPO system at 1.57 μm for integrated path DIAL measurement of atmospheric carbon dioxide, Appl. Phys. B-Lasers O.,
10   92, 295–302, 2008. 1500
Baldridge, A. M., Hook, S. J., Grove, C. I., and Rivera, G.: The ASTER spectral library version 2.0, Remote Sens. Environ., 113(4), 711–715, 2009. 1489, 1500, 1507
Bréon, F. M. and Henriot, N.: Spaceborne observations of ocean glint reflectance and modeling of wave slope distributions, J. Geophys. Res., 111, C06005, doi:10.1029/2005JC003343,
15   2006. 1510
Bréon, F. M., Maignan, F., Leroy, M., and Grant, I.: Analysis of hot spot directional signatures measured from space, J. Geophys. Res., 107(16), 4282–4296, 2002. 1489, 1503
Bufton , J. L., Hoge, F. E., and Swift, R. N.: Airborne measurements of laser backscatter from the ocean surface, Appl. Optics, 22(17), 2603–2618, 1983. 1489
20   Camacho-de Coca, F., Bréon, F. M., Leroy, M., and Garcia-Haro, F. J.: Airborne measurement of hot spot reflectance signatures, Remote Sens. Environ., 90(1), 63–75, 2004. 1505
Cox, C. and Munk, W.: Measurement of the roughness of the sea surface from photographs of the Sun's glitter, J. Opt. Soc. Am., 44(11), 838–850, 1954. 1489, 1505
Ehret, G., Amediek, A., Kiemle, C., Wirth, M., Fix, A., Houweling, S., and Behrendt, A.: Space-
25   borne Remote Sensing of the Greenhouse Gases CO_2, CH_4 , N_2O by Path Integrated Differential Absorption Lidar: A Sensitivity Analysis, Appl. Phys. B-Lasers O., 90, 593–608, 2008. 1489, 1491
European Space Agency (ESA): A-SCOPE – Advanced Space Carbon and Climate Observation of Planet Earth, Report For Assessment, ESA-SP1313/1, 2008. 1488, 1513

Airborne lidar reflectance measurements

A. Amediek et al.

Friedman, D.: Infrared Characteristics of Ocean Water (1.5–15 μm), Appl. Optics, 8, 2073–2078, 1969. 1489

Giordmaine, J. A. and Miller, R. C.: Tunable Coherent Parametric Oscillation in LiNbO3 at Optical Frequencies, Phys. Rev. Lett., 14(24), 973–976, 1965. 1498

5   Hapke, B., DiMucci, D., Nelson, R., and Smythe, W.: The Cause of the Hot Spot in Vegetation Canopies and Soils: Shadow-Hiding Versus Coherent Backscatter, Remote Sens. Environ., 58, 63–68, 1996. 1503

Justice, C. O., Townshend, J. R. G., Vermote, E. F., Masuoka, E., Wolfe, R. E., El Saleous, N., Roy, D. P., and Morisette, J. T.: An overview of MODIS Land data processing and product
10   status, Remote Sens. Environ., 83, 3–15, 2002. 1489, 1503, 1507

Kaasalainen, S., Kaasalainen, M., Mielonen, T., Suomalainen, J., Peltoniemi, J. I., and Näränen, J.: Optical properties of snow in backscatter, J. Glaciol., 52(179), 574–584, 2006. 1505

Kaasalainen, S. and Rautiainen, M.: Hot spot reflectance signatures of common boreal lichens,
15   J. Geophys. Res., 110, D20102, doi:10.1029/2005JD005834, 2005. 1505

Kalshoven Jr., J. E., Tierney Jr., M. R., Daughtry, C. S. T., and McMurtrey III, J. E.: Remote sensing of crop parameters with a polarized, frequency-doubled Nd:YAG laser, Appl. Optics, 34, 2745–2749, 1995. 1510

Lancaster, R. S., Spinhirne, J. D., and Palm, S. P.: Laser pulse reflectance of the ocean surface
20   from the GLAS satellite lidar, Geophys. Res. Lett., 32, L22S10, doi:10.1029/2005GL023732, 2005.

Larsson, H., Steinvall, O., Chevalier, T., and Gustafsson, F.: Characterizing laser radar snow reflection for the wavelengths 0.9 and 1.5 μm, Opt. Eng., 45, 116201-1–116201-11, 2006. 1514

25   Liang, S. L., Fang, H. L., Chen, M. Z., Shuey, C. J., Walthall, C., Daughtry, C., Morisette, J., Schaaf, C., and Strahler, A.: Validating MODIS land surface reflectance and albedo products: methods and preliminary results, Remote Sens. Environ., 83, 149–162, 2002. 1503

Meister, A., Fix, A., Flentje, H., Wirth, M., and Ehret, G.: TropOLEX: A New Tuneable Airborne Lidar System for the Measurement of Tropospheric Ozone, 6th International Symposium on
30   Tropospheric Profiling, Leipzig, Germany, 14–20 September 2003, 233–235, 2003. 1498

Menzies, R. T., Tratt, D. M., and Hunt, W. H.: Lidar In-space Technology Experiment measurements of sea surface directional reflectance and the link to surface wind speed, Appl. Optics, 37(24), 5550–5559, 1998. 1489

Airborne lidar reflectance measurements

A. Amediek et al.

Tang, C. L., Bosenberg, W. R., Ukachi, T., Lane, R. J., and Cheng, L. K.: Optical parametric oscillators, IEEE, Proceedings, 80(3), 365–374, 1992. 1498

Twomey, S. A., Bohren, C. F., and Mergenthaler, J. L.: Reflectance and albedo differences between wet and dry surfaces, Appl. Optics, 25, 431–437, 1986. 1514

5   Woessner, P. and Hapke, B.: Polarization of Light Scattered by Clover, Remote Sens. Environ., 21, 243–261, 1987. 1510

Airborne lidar reflectance measurements

A. Amediek et al.

Title Page	
Abstract	Introduction
Conclusions	References
Tables	Figures

◄◄	►►
◄	►
Back	Close

Full Screen / Esc

Printer-friendly Version

Interactive Discussion

Table 1. Technical Parameters of the system.

Transmitter	
wavelength	1573 nm
bandwidth	0.2 nm FWHM
energy per pulse	5 mJ
repetition rate	10 Hz
source	Nd:YAG pumped KTP-OPO system
beam divergence (full width)	3 mrad
Receiver	
telescope type	Cassegrain, 35 cm diameter
detector	InGaAs PIN (1 mm active area diam.)
field of view (full width)	4 mrad
data acquisition	12-bit, 400 MHz digitizer
detector/preamplifier bandwidth	4 MHz
Geometry	
down-looking, with off-nadir angle	1.2° (to forward direction)
laser spot diameter on ground	5–9 m (depending on flight altitude)
distance between two spots	8–10 m (depending on speed)
Platform	
aircraft	Cessna Grand Caravan 208B
ground speed	290–360 km/h
aircraft to ground distance	1.5–3 km
possible non-stop flight range	>1000 km

Table 2. Instrumental noise analysis results with respect to all quantities derived from the measurement data.

Quantity	Basis	Precision (RMS)
target distance	–	1 m
TROPOLEX reflectivity ρ	original	1.9%
	1-D upscaled (100 m)	0.6%
absolute reflectance ρ^*	original	$0.003\,\mathrm{sr}^{-1}$
	1-D upscaled (100 m)	$0.001\ \mathrm{sr}^{-1}$
reflectivity difference $(\delta\rho/\rho)_{10\,\mathrm{m}}$	original	2.7 percentage points
	1-D upscaled (100 m)	0.24 percentage points
A-SCOPE CO_2 error	1-D upscaled (100 m) and averaged aver 350 measurements	0.02 ppm (0.005%)

Table 3. Minimim and maximum reflectivity differences $(\delta\rho/\rho)_{10\,m}$ found in the collected data set; RMS values for 50-km-sections.

RMS$^{50\,km}[(\delta\rho/\rho)_{10\,m}]$	original	1-D up-scaled
minimum	13%	2.2%
maximum (snow free)	24%	4.1%
maximum (partly snow covered ground)	54%	10%

Table 4. A-SCOPE configuration parameters assumed for the retrieval error simulation.

Parameter	value
Platform altitude	400 km
Platform speed projected on ground	circa 7.2 km/s
Laser pulse operation	50 Hz double pulses
On/off time separation	250 μs
Averaging interval	50 km
Averaged pulse pairs	350
Laser footprint	gaussian, 38 m FWHM
Assumed spatial on-off mismatch (worst case)	10 m
CO_2 total column optical depth	$\Delta\tau = 1$
CO_2 column mixing ratio	380 ppm

Fig. 1. TROPOLEX system installed on the DLR research aircraft Cessna Grand Caravan.
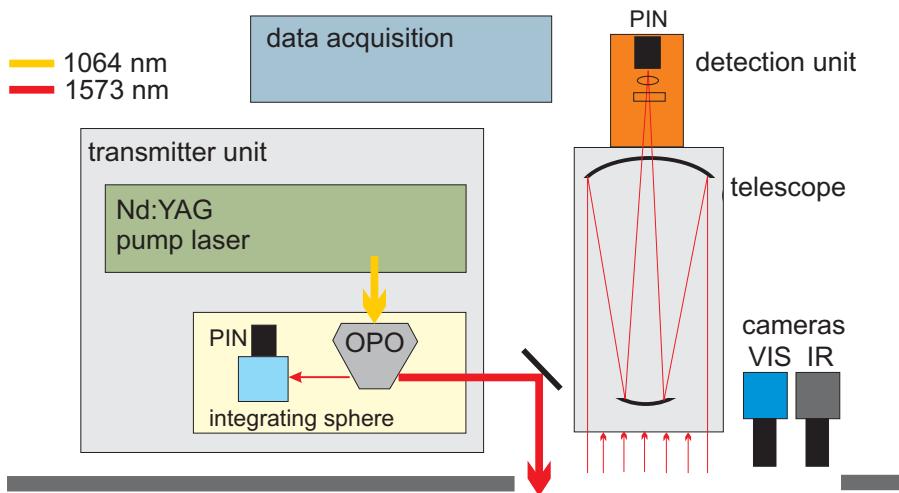
Fig. 2. TROPOLEX system layout for ground reflex measurements.

Fig. 3. Tracks of the performed flights in Central and Western Europe.
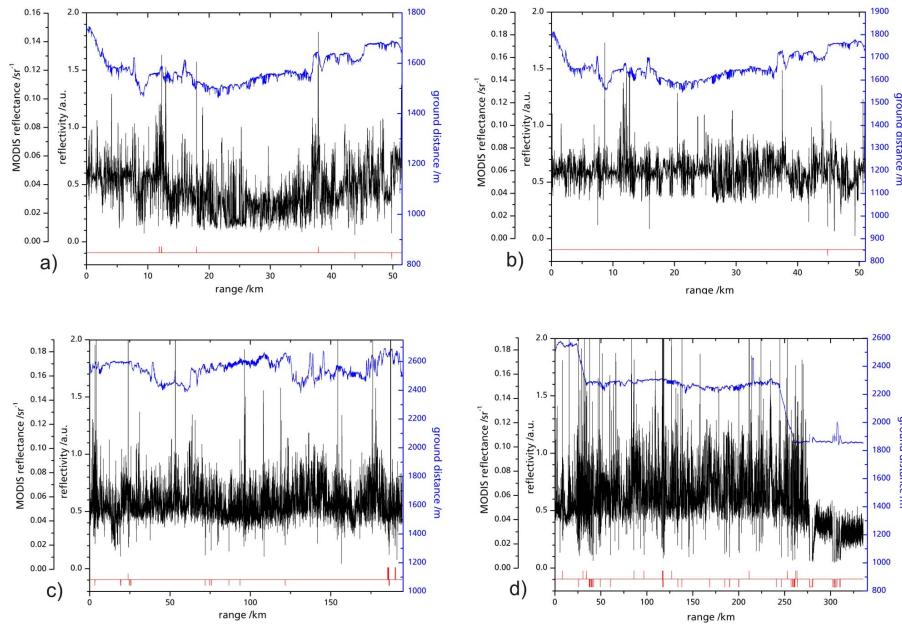
Fig. 4. Measurement data: **(a)** Southern Germany (April 2008, partly snow covered), **(b)** same route as in (a) (June 2008) , **(c)** Southern Germany (April 2008), **(d)** Northern Germany (April 2008).
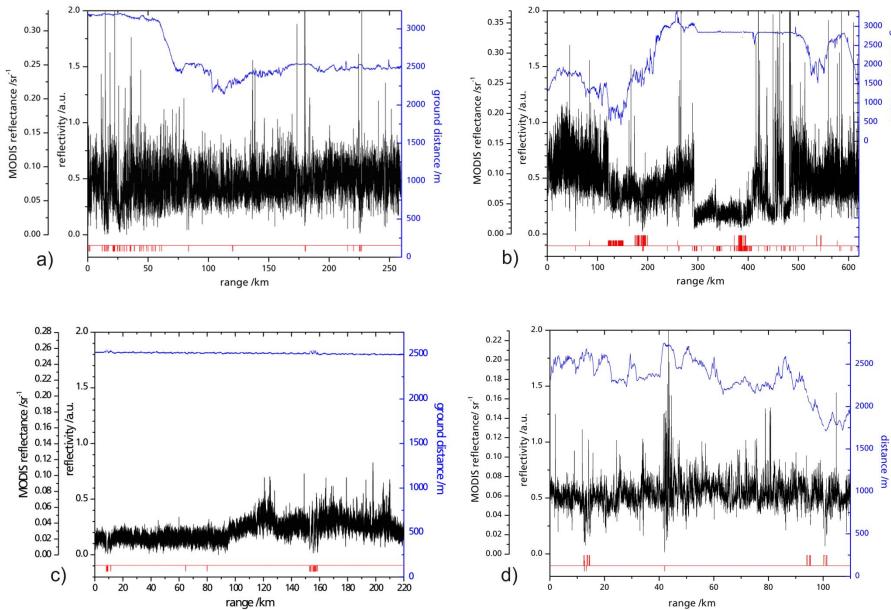
Fig. 5. Measurement data, June 2008: **(a)** Portugal, **(b)** Southern Spain (including Mediterranean Sea), **(c)** Mediterranean Sea, **(d)** Southern France.

Airborne lidar reflectance measurements

A. Amediek et al.
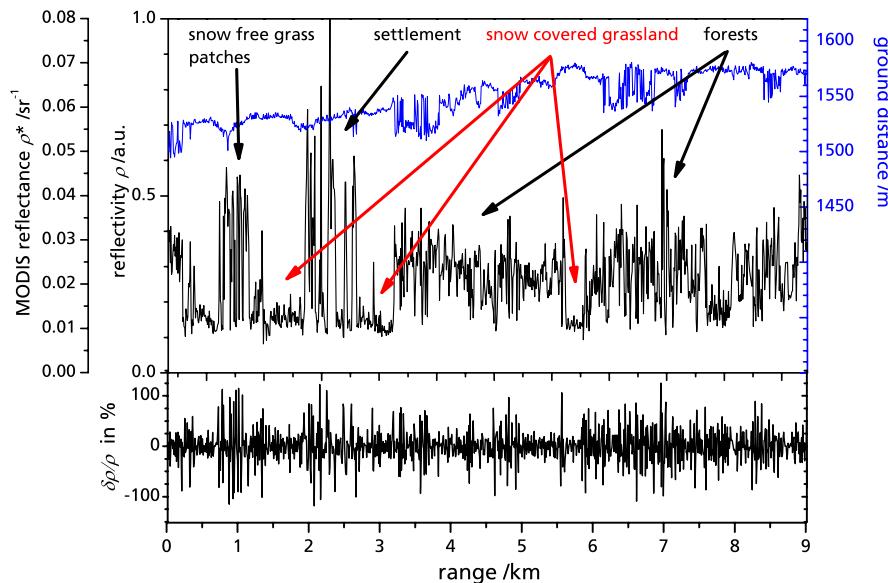
Fig. 6. 9-km-zoom taken from an April flight (Southern Germany); 10 m horizontal resolution, no footprint upscaling; upper panel: ground distance (blue) and TROPOLEX ground reflectivity (black); corresponding reflectances ρ^* taken from MODIS data as a second y-axis; lower panel: relative reflectivity differences $\delta\rho/\rho$; forest areas can be identified by the signatures in the ground distance.

Title Page

Abstract | Introduction

Conclusions | References

Tables | Figures

Back | Close

Full Screen / Esc

Printer-friendly Version

Interactive Discussion
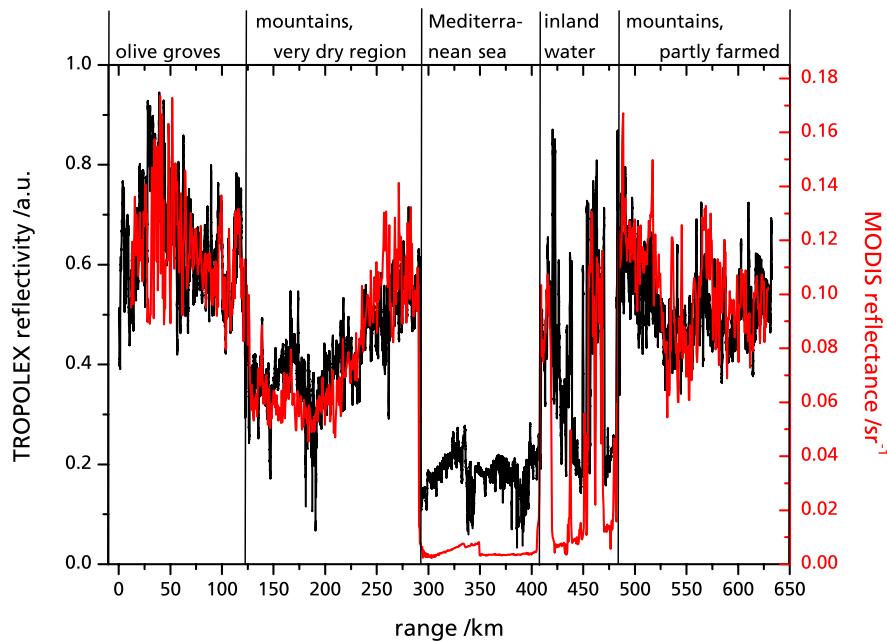
Fig. 7. Flight leg in Southern Spain (June 2008): TROPOLEX (500 m averages) and MODIS data (500 m pixel size).

Printer-friendly Version

Interactive Discussion
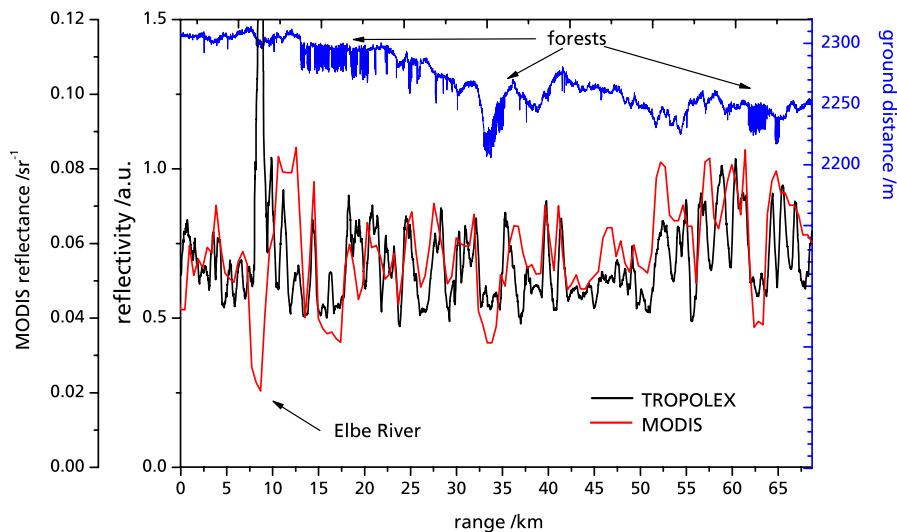
Fig. 8. Zoom into data from Northern Germany (April 2008): TROPOLEX (500 m averages) and MODIS data (500 m pixel size); forests alternating with agricultural fields just before the vegetation period (forests can be identified by the signatures in the ground distance).
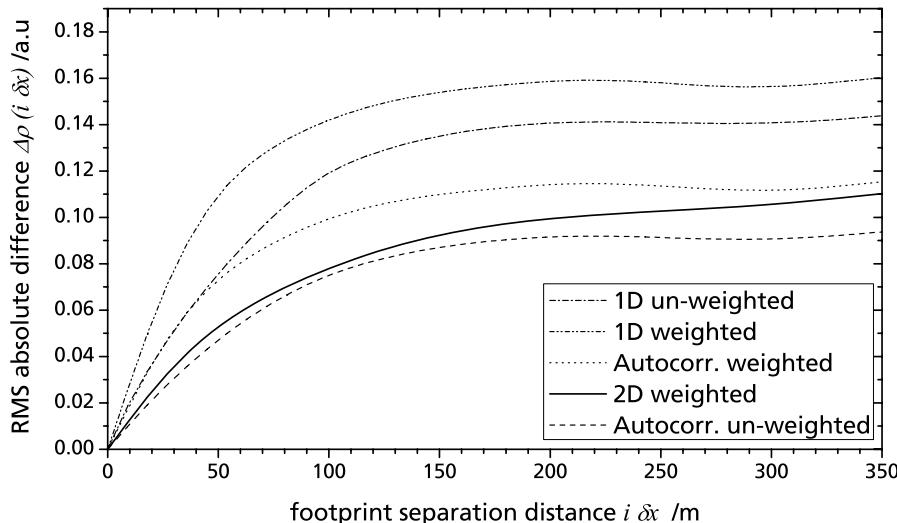
Fig. 9. Different upscaling approaches (100 m footprint diameter, un-weighted and gaussian weighted with 38 m FWHM) on the basis of 1-D measurement data compared to 2-D data (solid line, obtained by a special flight pattern).
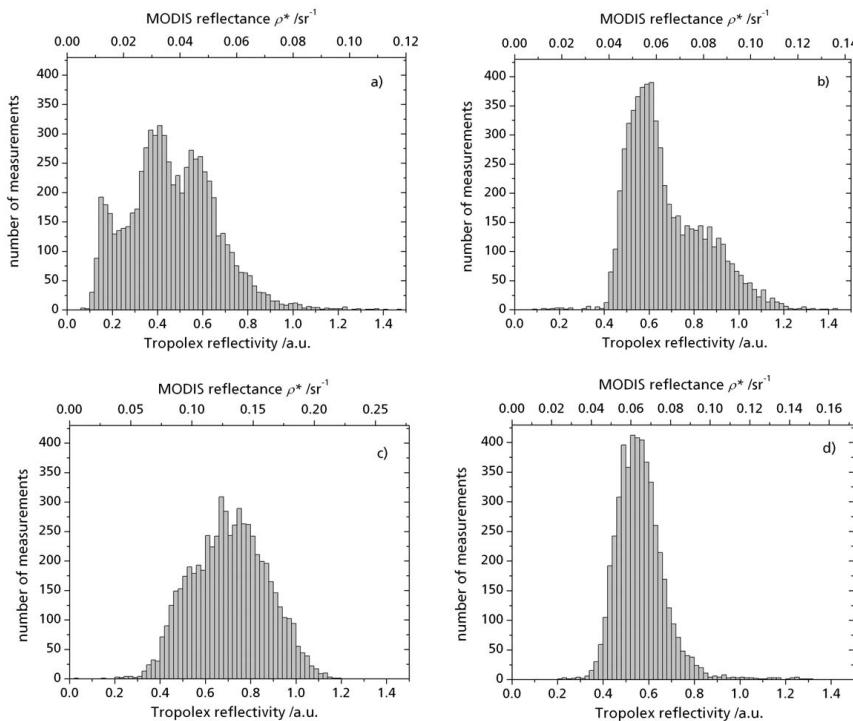
Fig. 10. Histograms of reflectivites ρ measured by TROPOLEX taken from different regions in Europe (50-km sections each): **(a)** Southern Germany (April), **(b)** Northern Germany (April), **(c)** Spain, olive groves (June), **(d)** Southern France (June).
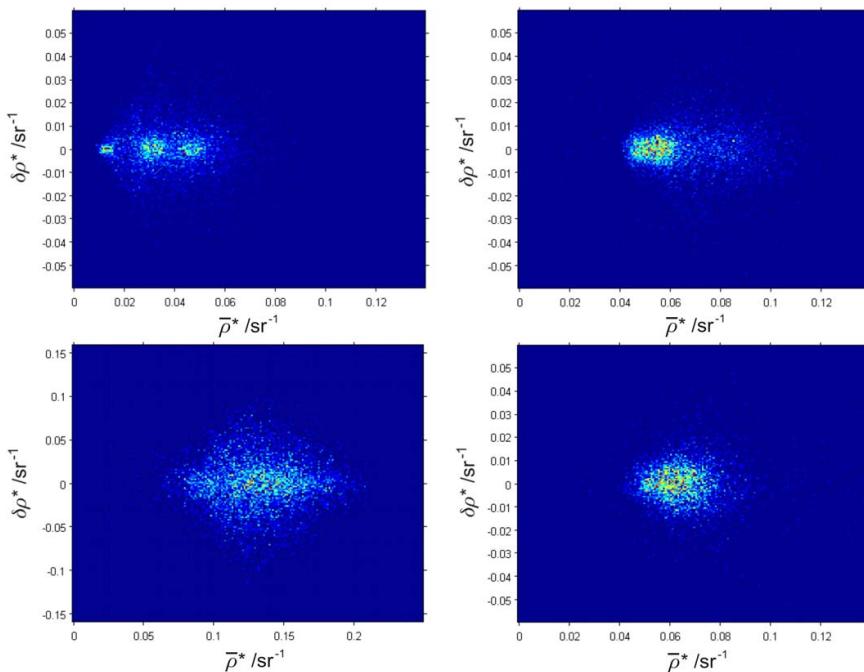
Fig. 11. Histograms of the absolute reflectance differences $\delta\rho^* = \rho_i^* - \rho_{i+1}^*$ dependent on the respective absolute mean reflectance $\overline{\rho}^* = (\rho_i^* + \rho_{i+1}^*)/2$ on the basis of the same data as used in Fig. 10 (absolute values base on the MODIS calibration according to Sect. 5).
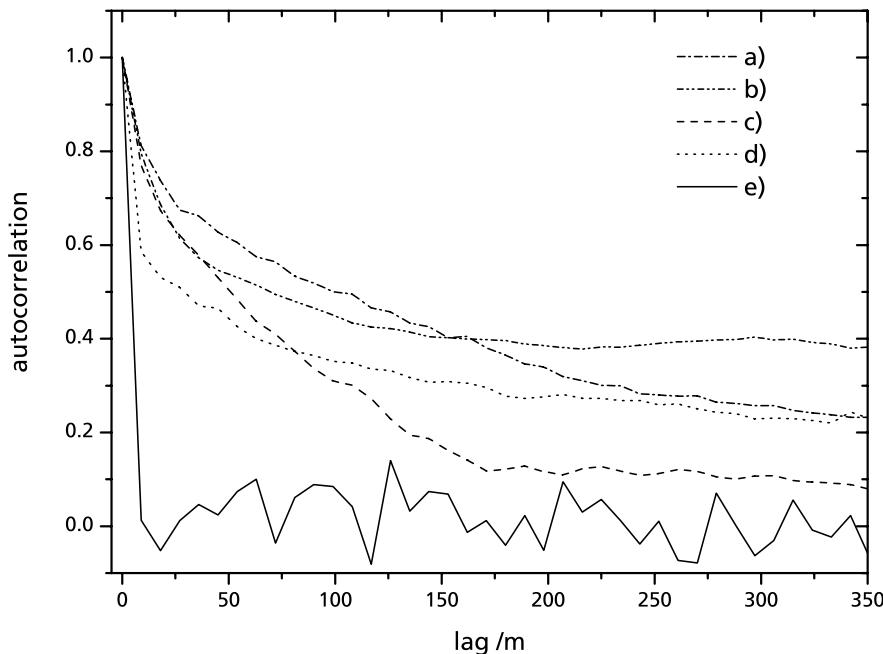
Fig. 12. Autocorrelations of the (non-up-scaled) reflectivites ρ from different regions: **(a)** Northern Germany (agricultural fields – large structures); **(b)** Southern Germany (forests, fields – small strucures); **(c)** Southern France (forests, fields – small strucures); **(d)** Southern Spain (olive groves – fine structures); **(e)** open sea.
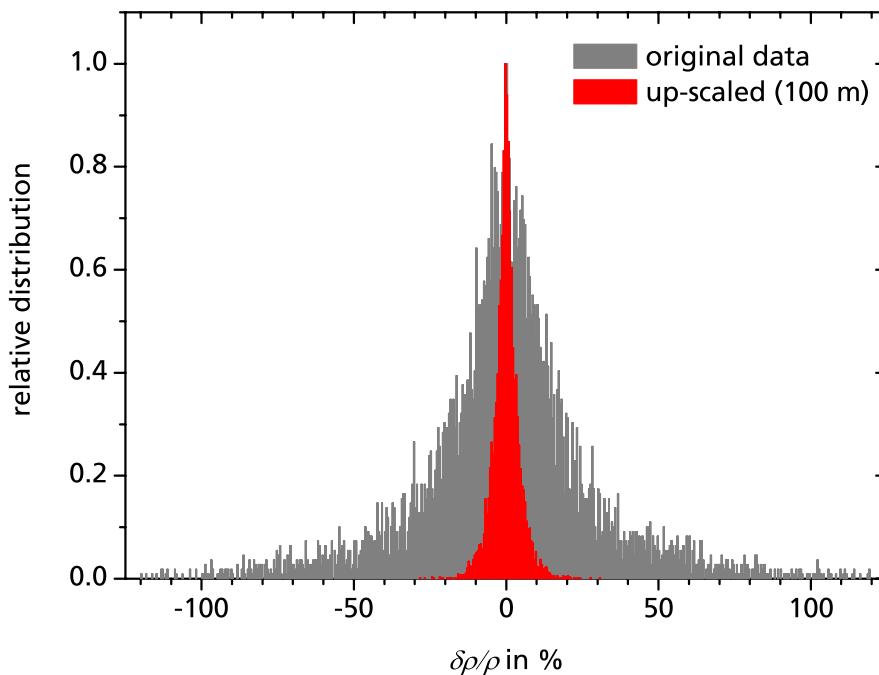
Fig. 13. Distribution of the relative reflectance differences $\delta\rho/\rho$ (per 10 m) for a 50-km-flight leg (about 6500 measurements) in Southern Germany: the RMS of the non-upscaled data is 29.9%, of the up-scaled data 4.4%; the distribution is almost symmetrical, the mean is 0.004% (bin size: 0.5%).

Title Page

Abstract | Introduction

Conclusions | References

Tables | Figures

◀◀ | ▶▶

◀ | ▶

Back | Close

Full Screen / Esc

Printer-friendly Version

Interactive Discussion
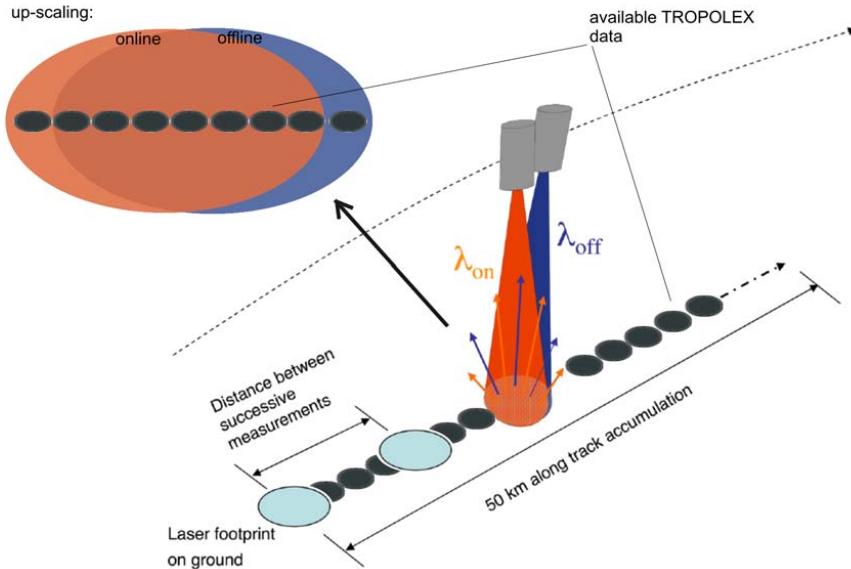
Fig. 14. Illustration of the A-SCOPE retrieval error calculation using TROPOLEX ground reflectance data.

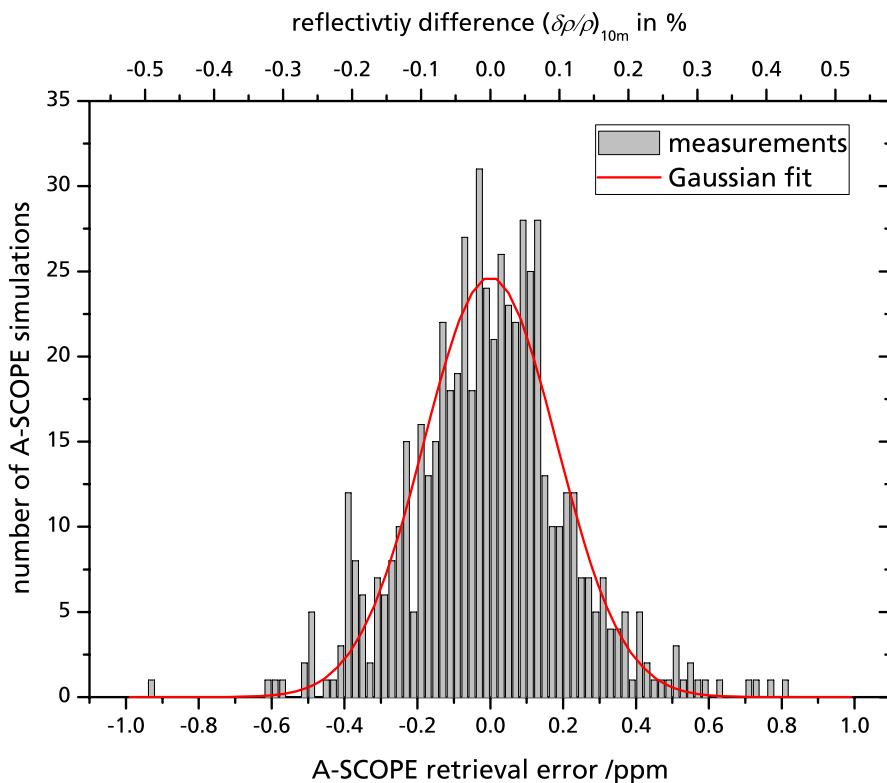**Airborne lidar reflectance measurements**

A. Amediek et al.

Fig. 15. Histogram for A-SCOPE retrieval errors (bin size: 0.02 ppm) and corresponding relative reflectance differences on the basis of all data collected during this project.